Noname manuscript No.
(will be inserted by the editor)

# Importance of Weighting Full-Field Displacement Components when Fitting Material Parameters

Charles F. Jekel* ** · Martin P. Venter · Gerhard Venter · Raphael T. Haftka

Received: date / Accepted: date



** Lawrence Livermore National Laboratory is operated by Lawrence Livermore National Security, LLC, for the U.S. Department of Energy, National Nuclear Security Administration under Contract DE-AC52-07NA27344.

C. F. Jekel *corresponding author*
Department of Mechanical and Aerospace Engineering, University of Florida, Gainesville, FL 32611, USA
E-mail: jekel1@llnl.gov
Present address: of C. F. Jekel
Lawrence Livermore National Laboratory, L-227, PO Box 808, Livermore, CA, 94551, USA

M. P. Venter
E-mail: mpventer@sun.ac.za
Department of Mechanical and Mechatronic Engineering, Stellenbosch University, Private Bag X1, Matieland, 7602, South Africa

G. Venter
E-mail: gventer@sun.ac.za
Department of Mechanical and Mechatronic Engineering, Stellenbosch University, Private Bag X1, Matieland, 7602, South Africa

R. T. Haftka
Department of Mechanical and Aerospace Engineering, University of Florida, Gainesville, FL 32611, USA

Supplementary material available online that includes data and videos covered in this paper: `https://github.com/cjekel/inv_bubble_opt`

Abstract A methodology is presented to fit material parameters in finite element (FE) models using full displacement field data. Four bulge inflation tests were performed on a PVC-coated polyester material. Digital image correlation (DIC) was used to capture the full displacement field of the material. An inverse analysis was set up to find material parameters in a FE model which best matched the full displacement field of the experimental test. Three different objective functions were considered to quantify the discrepancy between the FE model and experiments. The first function only matched the maximum out-of-plane deflection, representative of an experiment with a single point deflection measure. The other functions consider matching the numerical model to the full three dimensional displacement field, where one function considers a weighted scheme to balance the order of magnitude difference between in-plane and out-of-plane displacements. The resulting material parameters were heavily dependent upon which objective function was chosen. The best parameters are thought to come from the weighted objective function considering the full-field data, which matched the in-plane displacements better than the other objective functions.

Keywords Inverse analysis · Objective functions · material parameter identification · bulge inflation test

## 1 Introduction

The finite element (FE) method is an important tool used to design membrane structures. These FE models rely on the efficacy of material models for design insight, and unfortunately selecting appropriate material parameters to represent complex behavior can be difficult. This is especially true for materials like coated fabrics, which typically consist of a vinyl polymer coating over woven yarns bundled from several fibers. Inverse analyses, or iterative schemes for FE model updating (FEMU) have been used to find material parameters from complex load cases. In this paper, three different objective functions were investigated with FEMU to estimate material parameters from bulge inflation tests on PVC-coated polyester. Objective function refers to how the discrepancy between the FE model and test data is quantified, and material parameters are typically selected to minimize this function. The objective function has an important effect on the material parameters selected using this type of inverse analysis (Zhan et al., 2011; Jekel et al., 2019; Tam, 2020).

PVC-coated polyester is a coated textile. It's most commonly modeled as a continuous, homogeneous, orthotropic material (Shaw et al., 2010), which can have large material direction dependent strength due to the warp-to-fill stiffness ratio (Dinh et al., 2017). The typical weave has the warp yarns pulled taut, while the fill yarns are woven in-between the warp yarns. The fill yarns run orthogonal to the warp yarns. Various non-linear models have been used in an attempt to better describe the behavior of the material. Galliot and Luchsinger (2009) proposed a non-linear material model based on the load ratio between the material warp and fill directions. Ambroziak and Kłosowski (2014) used a piecewise linear orthotropic model, and Jekel et al. (2017) used polynomials to describe the non-linear elastic behavior of the material.

Biaxial tests are commonly used to characterize material parameters for structural membrane materials (Stranghöner et al., 2016). Several studies have used bulge

(or bubble, or membrane) inflation tests to induce an equal biaxial load on the material. These bulge tests typically involve inducing a pressure on one side of a circularly clamped membrane material. Reuge et al. (2001) performed these bulge inflation tests on a rubber material and outlined the assumptions that lead to an equal biaxial load occurring at the apex of the deflected membrane material. Sasso et al. (2008) provides a good review of how bulge inflation tests compare to other forms of tension tests. Much of these early bulge inflation tests only recorded the apex height (Rachik et al., 2001; Charalambides et al., 2002). More recent bulge inflation tests have adopted the use of 3D digital image correlation to measure the entire surface deformation of the membrane material (Machado et al., 2012). Tonge et al. (2013a) stated that the full displacement field allows for the determination of in-plane material directions and was later used to calibrate a material model for human skin.

It is often the case that FEMU is used to calibrate material parameters by formulating and inverse problem to match a numerical model to some physical experiment (Lovato et al., 1993; Cailletaud and Pilvin, 1994; Drass and Schneider, 2016). The process can be generalized by using optimization to find parameters in a FE model which minimize the discrepancy between the model and experimental data (Asaadi et al., 2017). In a forward problem, parameters can be directly inferred from an experimental test. While an inverse problem iteratively updates the FE model to find parameters that best match an experimental response (Lee et al., 2019). This process is often referred to as model calibration. The FE model must be accurate enough to get reasonable parameters when using FEMU. Oversimplified assumptions or incorrect boundary conditions may result in non-sensible parameters. As such, a validation step is necessary to ensure the parameters calibrated with FEMU are sensible before being used in other practical tasks. We refer the reader to strategies by Oh et al. (2016) and Son et al. (2020) to statistically improve the accuracy of FE models to both blind and known uncertainties. Additionally, there may be some cases where unknown boundary conditions may be included into the optimization formulation of the material calibration problem as performed by van Rensburg et al. (2018).

Model calibration can be performed using deterministic or probabilistic methods (Lee et al., 2019). A deterministic model calibration does not include the measurement uncertainty, while probabilistic method can account for both model and experimental uncertainty. Jung et al. (2016) stated that models calibrated deterministicly do not account for material uncertainty, and thus may result in unreliable solutions. The uncertainty of the experiments needs to be quantified in order to calibrate material models probabilistically. Unfortunately, DIC displacement field data is typically treated as a black box where uncertainties are not well understood. The bulge inflation test is particularly challenging having out-of-plane displacements on the curved material surface. While it may be more reliable to calibrate the material model parameters using a probabilistic method, this work uses a deterministic method because the uncertainty due to DIC errors of the displacement measurements is currently unknown. However, the experimental measurements are made available, so that a probabilistic calibration can be performed in the future.

There are many different choices of possible objective functions to calibrate material models. Zhan et al. (2011) proposed the EARTH method to calibrate model parameters into phase, magnitude, and slope errors from time history data. A single DIC bulge inflation test may generate over a hundred thousand unique time

histories. In order to apply EARTH, each of these time histories would need to be broken into their respective errors and treated as separate objective functions in a multi-objective optimization. This process to compute the objective functions may be computationally expensive with full-field data.

The previous studies (Rachik et al., 2001; Charalambides et al., 2002) used only the height to determine material parameters from bulge inflation tests. Tonge et al. (2013b) only used a single stress resultant as the cost function for calibration. Machado et al. (2012) used curvatures to determine a stress tensor from bulge inflation tests to infer material parameters for an elastic material. While these previous methods work well for a planar isotropic material, they are difficult to extend to a directional dependent woven textile like PVC-coated polyester. Additionally, it is unclear how important normalization will be to the objective function when calibrating to multiple displacement components. This work will calibrate a linear orthotropic material model from bulge inflation tests. Calibrating material parameters using the bugle height (displacement at maximum deflection) will be compared to not only the full displacement field, but also with weighted (or normalized) displacements.

Jekel et al. (2016) showed that it was possible to use the displacement field of a bulge test to select parameters for a non-linear orthotropic material model using simulated experimental data. Jekel (2016) then used this process on polynomial displacement fields fitted to experimental data at selected inflation pressures. These polynomial surfaces introduce an extra layer of error in the material parameters, as the error in the polynomial fit was not properly accounted for. While previous work used a surrogate model to represent the experimental data, this work will find material parameters by fitting the full experimental displacement field directly. A new approach is described which allows for any data point in the experimental displacement field be compared to a FE model, for any initial surface location and inflation pressure.

Jekel et al. (2016) considered the discrepancy in the $x$,$y$ and $z$ displacements fields. When only the $z$ displacements were utilized, there appeared to be multiple equivalent displacement solutions for a given material parameter set, possibility hinting that the FEMU problem was undetermined. However, with the inclusion of $x$ and $y$ displacements, there appeared to be a unique set of material parameters to represent the entire displacement field. While the previous work only considered numerical results, this work now considers experimental data. The experiments show that the out-of-plane deformations were an order of magnitudes larger than the in-plane displacements, which we believe this weighting may play an important role when calibrating parameters to real experimental data.

This paper is organized into five sections: 1) Introduction, 2) Methods, 3) Results, 4) Discussion, and 5) Conclusion. The Methods section details the process used to obtain material parameters from the bulge inflation tests. Subsections are used within the method section to draw attention to experimental test setup, FE model, mathematical discrepancy between the experiment and FE model (objective function), and optimization procedure. The results section is split into three parts to separate the isotropic material parameters, orthotropic material parameters, and the cross validation study. The discussion goes on to focus on the orthotropic results, and conclusions are presented.

## 2 Methods

This section describes the FEMU method utilized in this research to understand how the objective function affects resulting material parameters. The bulge inflation tests were performed using DIC on PVC-coated polyester.[1] This experiment outputs full-field displacement data ($\Delta x, \Delta y$, and $\Delta z$) from a flat circular piece of membrane material. A FE model was created replicating the boundary conditions of the bulge inflation tests. Three different objective functions are described. Each objective function represents a different method to quantify the difference between the experimental data and FE model. One quantity considers only the height of the bulge experiment, the other considers the full-displacement field, and the last considers a weighted variant of the full-displacement field. Then the optimization process to perform the inverse analysis is briefly described, which results in linear orthotropic material parameters.

### 2.1 Experimental tests

The bulge inflation tests involve clamping a sample of membrane material into a circular clamp. Pressure is then induced on one side of the material. The material deflections were recorded using DIC. The DIC system used was the StrainMaster with DaVis (LaVision GmbH, 2014), which was capable of syncing the inflation pressure with the recorded images. A visual representation of a bulge inflation test is provided in Figure 1.

Four bulge inflation tests were performed at Stellenbosch University in South Africa. Details of the process and test fixture are found in section 5.1 of (Jekel, 2016). The diameter of the circular bulge test was 200 mm. The PVC-coated polyester tested was Mehler Texnologies VALMEX® 7318 (the same material tested in(Jekel et al., 2017)). Four samples of material were cut from the same roll, with each sample being a 250 mm square. Spray paint was added to the surface of each specimen, with a random pattern, to increase the surface contrast of the material for DIC processing. Each test was inflated from zero to three bar, by manually opening a compressed air valve to the bulge inflation test fixture. This resulted in each test being inflated at a unique load rate as seen in Figure 2. The internal pressure was recorded with a Festo SPTE-P10R-S4-V-2.5K pressure transmitter.

Full-field bulge inflation tests generated a large amount of data as shown in Table 1. The $xy$-plane was oriented with the surface of the material prior to inflation, with the $x$ direction occurring in the warp material direction, while the $y$ direction occurred in the fill material direction. The material was inflated in the $z$ direction. Here the largest test generated nearly two million data points, while the smallest test generated only two hundred thousand data points. Each data point represents a unique combination of inflation pressure $p$ and initial $x, y$ location. There are three deformations recorded for each data point, represented as separate $\Delta x, \Delta y$, and $\Delta z$ values.

The post-processing parameters relating to the DIC technique were changed from test to test which resulted in a different number of data points being captured on

[1] An online repository is available at `https://github.com/cjekel/inv_bubble_opt` which includes the source code to perform the inverse analysis, test data, and procedures to reproduce this work.

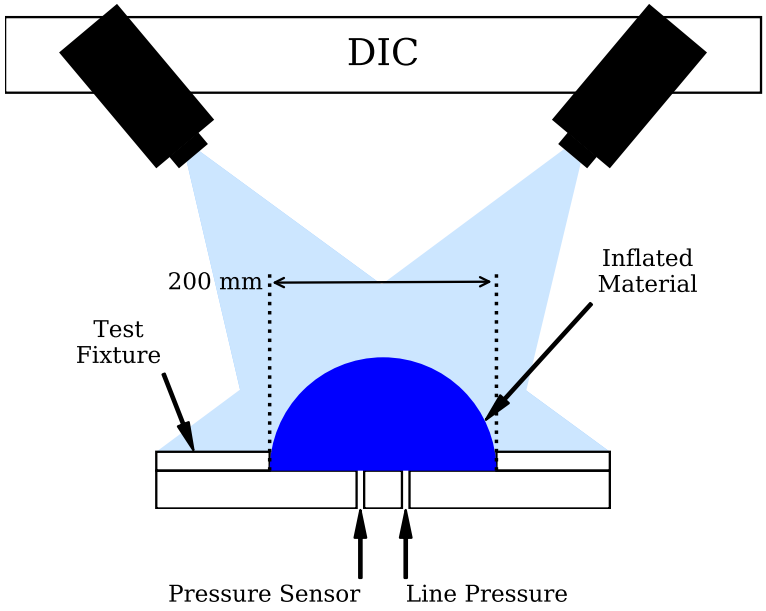


Fig. 1 Bulge inflation test overview.

Table 1 Number of unique $(x, y, p)$ data points from each test and inflation pressures.

| Test | # of data points |
|---|---|
| 1 | 1,836,961 |
| 2 | 729,718 |
| 3 | 1,201,509 |
| 4 | 289,312 |

the material specimen from test to test. The post-processing parameters include a window size, which is used to match the correlation between subsequent images. The size of the window directly influences the number of data points that occur on the material specimen. This window size needed to be changed from test to test because of variation in the random speckle pattern on the material. In an industrial application this variation can be controlled through the use of tools (e.g. multiple paint stencils) to produce a consistent pattern from test to test. A more consistent speckle pattern would allow for the same post-processing parameters, and a more consistent number of data points on the surface of the material specimen.

The DIC techniques were not perfect, as there are missing data points in some of the tests which is a common phenomenon with these techniques. This happens when correlations are lost between images, and becomes more evident with larger deflections. The tested PVC-coated polyester had a glossy finish, which would cause reflections to move on the surface of the material as the material deformed out-of-plane. These moving reflections would cause the DIC technique to lose correlation of patterns with subsequent images, resulting in ”holes” on the post-processed images. Additionally, the severity of missing data varies from test to test. Figure 3 shows

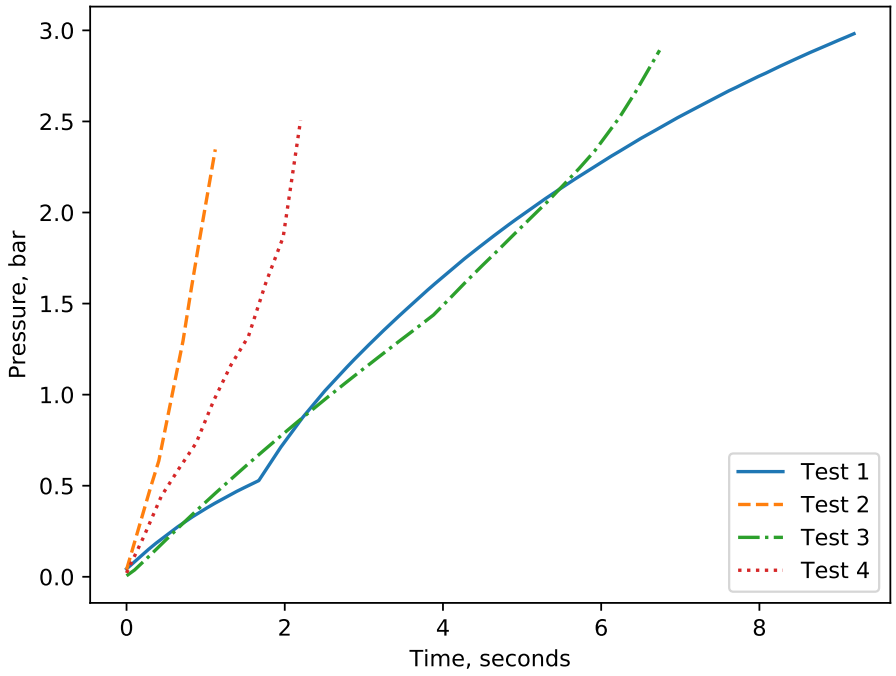


Fig. 2 Pressure time curves from each bulge inflation test.

each $x,y$ data point at the last inflation pressure of each test, where each colored pixel is a DIC data point. While Tests 1 and 2 have the highest density of data points, Test 1 doesn't have any missing data points while Test 2 has several small holes on the surface of the material. The worst of the missing data occurs with Test 3, which has large holes on one quarter of the test. Test 4 only has two small holes on the surface of the data, and also has the least number of $x,y$ data points on the surface of the material.

For a recorded pressure, the experimental test data includes a matrix of values, where each column represents either the initial position ($x$, $y$, $z$), or the deformation in each direction ($\Delta x, \Delta y$, $\Delta z$). A single row of this matrix represents a single point in three dimensional space on the surface of the material. The $k^{\text{th}}$ point was initially at $x_k$, $y_k$, and $z_k$ prior to inflation. Then for a given pressure, the point is physically located at $x_k + \Delta x_k$, $y_k + \Delta y_k$, and $z_k + \Delta z_k$ in the three-dimensional space. Videos for each test are included as supplementary material to help visualize the experimental data. There is a video for each test showing the $\Delta x, \Delta y$, or $\Delta z$ deflections of the material. There is also a video showing the three-dimensional shape of the material ($[x_k + \Delta x_k, y_k + \Delta y_k, z_k + \Delta z_k]$). Take note that the videos are not in a real physical scale. The videos show the raw data points captured from the experimental test, where each data point is used in the calibration process of the material.

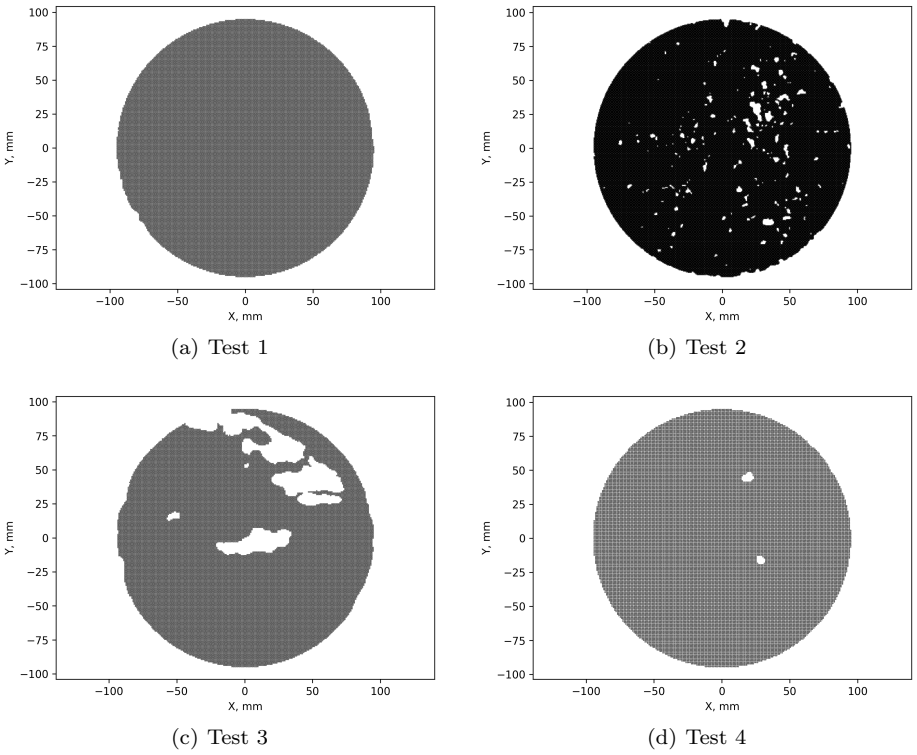


(a) Test 1 (b) Test 2

(c) Test 3 (d) Test 4

Fig. 3 Plots of the $x$,$y$ data points of each bulge inflation test. The darker color is related to having a higher density of data points.

## 2.2 Finite Element model

An implicit non-linear FE model was constructed in ABAQUS replicating the boundary conditions of the bulge inflation test. The material is modeled as a membrane material. Clamped boundary conditions are applied to the edge of the material. A surface pressure is applied as a function of time to inflate the membrane material. A non-linear model is needed to describe the geometric non-linearity as Sheplak and Dugundji (1998) demonstrated, with large deflections the center load displacement curve quickly transitions from linear to non-linear as the mid-plane force quickly grows with respect to geometry.

The FE model uses an implicit solver, with 201 load steps between zero and three bar. Each load step uses adaptive time stepping. The adaptive time stepping allows the model to solve a single load-case in one step, or cut back to smaller increments if needed. Over 900 linear Q4 membrane elements are used to represent the surface of the material. The displacement field at the nodes are exported to be compared to the experimental tests for a candidate set of material parameters.

The displacement field of the FE model needs to be available at various pressures of the current experimental data and potential future data. Either load steps can be added to the FE model at the exact experimental pressures, or the displacement field of the FE model can be interpolated at the observed experimental pressures.

Interpolation was chosen since it didn't involve manually editing the input deck for each experiment. Specifically linear interpolation was used to evaluate the FE model's displacement at the nodes for the exact pressures of the experimental test. The displacement of the FE model can be expressed as $\Delta(x,y,p)$. The experimental data records the displacements at the initial position $x,y$ and pressure $p$. Linear interpolation is used to solve the displacement field $\Delta(x,y,p)$ at the exact experimental pressure $p$ by interpolating the nodal FE solution at the two nearest computed pressures as

$$\frac{\Delta(x,y,p)-\Delta(x,y,p_1)}{p-p_1}=\frac{\Delta(x,y,p_2)-\Delta(x,y,p_1)}{p_2-p_1} \tag{1}$$

where $p_2$ and $p_1$ represent the nearest pressures of the FE model's load steps. The advantages of this interpolation scheme is that both the FE deck and post-processing routines do not need to be altered in order to obtain displacements of the model for any obscure pressure from future experiments.

Overall, the linear interpolation scheme proved very accurate when interpolating between the FE model load steps. The linear interpolation accuracy was compared to FE models with load steps halfway in-between the previous 201 load steps (representing the worse possible interpolation case). The linear interpolation error was negligible, with the interpolation error following on the order of single precision ($10^{-8}$ mm) numerical noise. This level of noise was the same level of precision used by the FE model. The maximum possible error from this interpolation scheme has a hard bound as defined by Conte and Boor (1980). For any given $p_2$ and $p_1$, the maximum error from interpolation in deflection is bounded by

$$|E|_{\max}=\frac{(p_2-p_1)^2}{8}\max\left(\left|\frac{\partial^2\Delta}{\partial p^2}\right|\right). \tag{2}$$

Linear isotropic and orthotropic material models were investigated. An isotropic model with one unknown parameter (stiffness modulus $E$), and an isotropic model with two unknown parameters (stiffness modulus $E$ and the shear modulus $G$) were considered. The orthotropic model was simplified as a three parameter model, with parameters for the stiffness moduli ($E_1$ & $E_2$), and the shear modulus ($G_{12}$). The one parameter isotropic model and the orthotropic model use a Poisson's ratio of 0.24 as measured in (Jekel et al., 2017). We believe that our experimental setup would require through thickness measurements in order to accurately characterize the Poisson's ratio. There are additional compelexities While previous work of Jekel et al. (2017) used non-linear material models to characterize the PCV-coated polyester, this work used linear material models which seemed sufficient to match the load-displacement response observed in the bulge experiments.

The displacement field of the FE model for an orthotropic material model at 2.0 bar is shown in Figures 4 through 6. The maximum $\Delta z$ value is about ten times larger than the $\Delta x$ or $\Delta y$ values. Radial Basis Functions (RBF) are used to interpolate the displacements from the initial $(x,y)$ node locations of the FE model to be evaluated at the experimental locations (Broomhead and Lowe, 1988). The RBFs are exact at the node locations, and result in a smooth displacement field from the linear four node FE elements. The InterpolateSimpleRBF object construct these RBFs to the full displacement field of the FE analysis. The RBFs were inspired by the SciPy rbf function (Virtanen et al., 2020).

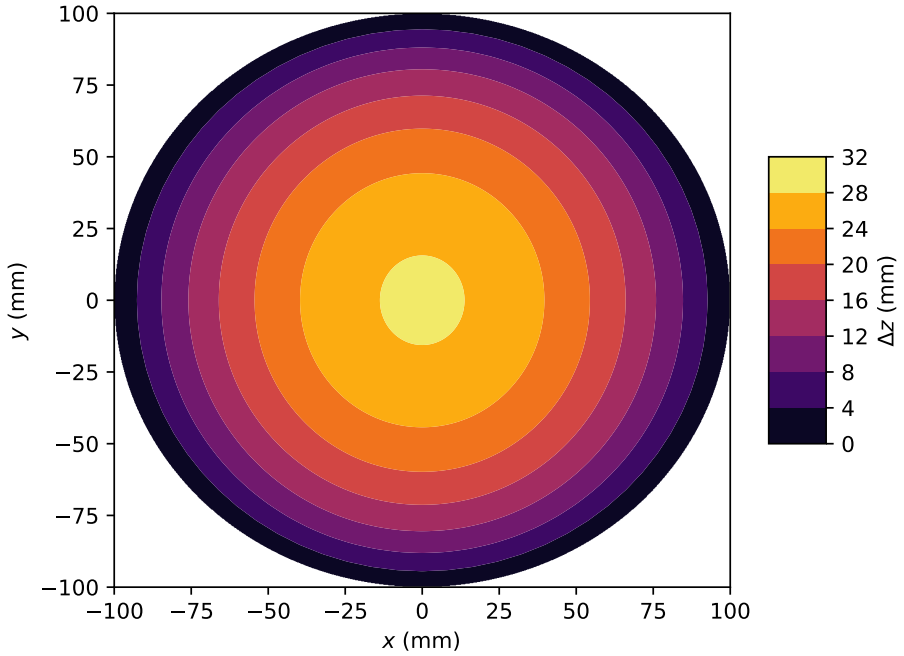


Fig. 4 Displacement $\Delta z$ of FE model at 2.0 bar with orthotropic properties $E_1 = 0.8$ GPa, $E_2 = 0.15$ GPa, $G_{12} = 0.025$ GPa, and $\nu_{12} = 0.24$.

### 2.3 Objective functions

The objective function is the mathematical quantity of interest which quantifies the discrepancy between the physical bulge inflation tests and the FE model. An optimization procedure minimizes the objective function to find the best set of material parameters. A simple objective function can be constructed which only minimizes the difference in $\Delta z$ displacement at the $(x = 0, y = 0)$ center of the membrane as

$$e_z(\boldsymbol{\beta}) = \sum_{i=1}^{n_p} |\Delta z(p_i)_t - \Delta z(p_i, \boldsymbol{\beta})_f| \tag{3}$$

where $n_p$ is the number of inflation pressures for from a given test. This is a $L^1$ norm between the experimental heights and observed heights.

Quantifying the difference between the full-field experimental data is more complicated than only considering a single point. Let the average absolute deviation between the $x$ displacement of the FE model and inflation test be denoted by $r_{\Delta x}(j, \boldsymbol{\beta})$ for the $j$ test and $\boldsymbol{\beta}$ set of material parameters. The $L^1$ deviations for the displace-

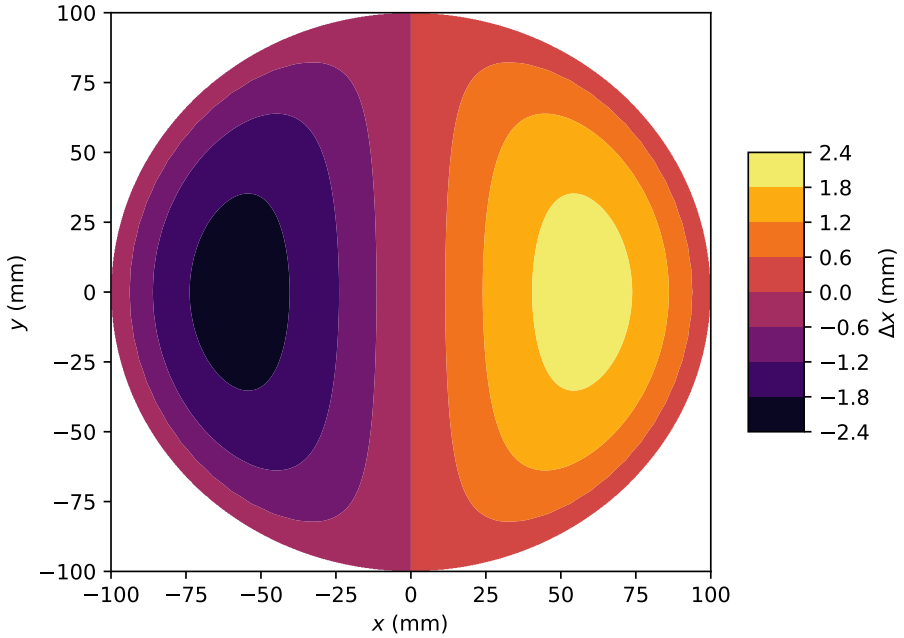


Fig. 5 Displacement $\Delta x$ of FE model at 2.0 bar with orthotropic properties $E_1 = 0.8$ GPa, $E_2 = 0.15$ GPa, $G_{12} = 0.025$ GPa, and $\nu_{12} = 0.24$. Note the symmetry about $x = 0$.

ment components are expressed as

$$r_{\Delta x}(j,\boldsymbol{\beta}) = \frac{1}{n_j}\sum_{i=1}^{n_j} |\Delta x(x_i,y_i,p_i)_t - \Delta x(x_i,y_i,p_i,\boldsymbol{\beta})_f| \tag{4}$$

$$r_{\Delta y}(j,\boldsymbol{\beta}) = \frac{1}{n_j}\sum_{i=1}^{n_j} |\Delta y(x_i,y_i,p_i)_t - \Delta y(x_i,y_i,p_i,\boldsymbol{\beta})_f| \tag{5}$$

$$r_{\Delta z}(j,\boldsymbol{\beta}) = \frac{1}{n_j}\sum_{i=1}^{n_j} |\Delta z(x_i,y_i,p_i)_t - \Delta z(x_i,y_i,p_i,\boldsymbol{\beta})_f| \tag{6}$$

where $n_j$ is the total number of data points in the $j$ test. A simple discrepancy is then formulated as the cumulation of the $L^1$ discrepancies in mm as

$$e(\boldsymbol{\beta}) = \frac{1}{n_t}\sum_{j}^{n_t} r_{\Delta x}(j,\boldsymbol{\beta}) + r_{\Delta y}(j,\boldsymbol{\beta}) + r_{\Delta z}(j,\boldsymbol{\beta}) \tag{7}$$

where $n_t$ is the total number of tests. The subscripts $t$ is for the physical inflation test data, while the subscript $f$ is from the FE model.

The formulation of $e$ considers the discrepancy in the $\Delta x$, $\Delta y$, and $\Delta z$ displacements to be of equal weight. This formulation could be problematic if the discrepancy in one displacement components dominates the others. In the bulge inflation test data, the $\Delta z$ component was roughly ten times larger than the in-plane ($x$ or $y$) components. This creates the potential for the $r_{\Delta z}$ discrepancies to be larger than

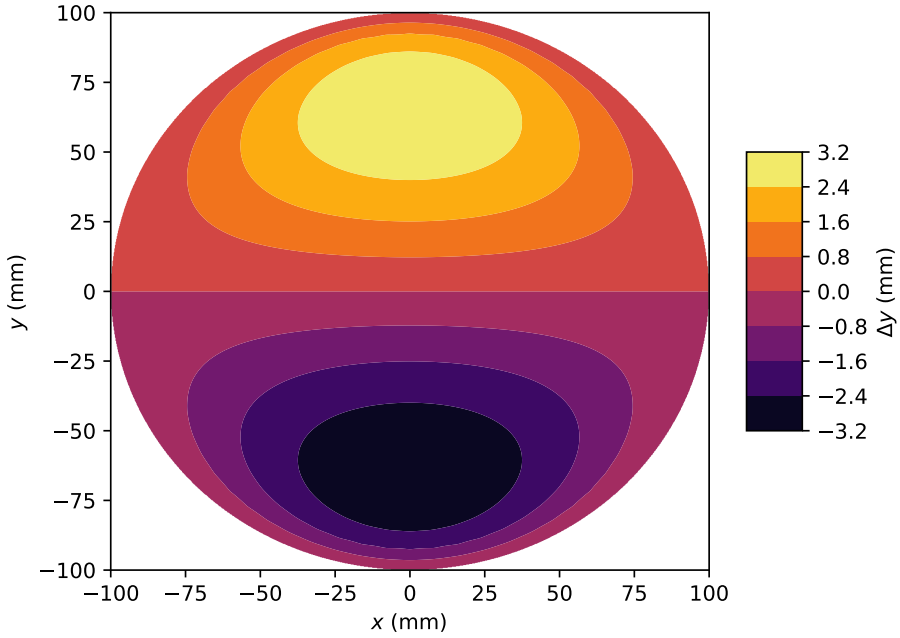


Fig. 6 Displacement $\Delta y$ of FE model at 2.0 bar with orthotropic properties $E_1 = 0.8$ GPa, $E_2 = 0.15$ GPa, $G_{12} = 0.025$ GPa, and $\nu_{12} = 0.24$. Note the symmetry about $y = 0$.

the other two directions, because the $\Delta z$ values have the potential to be at least ten times larger than $\Delta x$ or $\Delta y$.

A second objective function is proposed as $e_w$ to deal with the imbalance between the maximum in-plane and out-of-plane displacements. The function is just a slight modification of $e$, and is expressed as

$$e_w(\boldsymbol{\beta}) = \frac{1}{n_t}\sum_{j}^{n_t} r_{\Delta x}(j,\boldsymbol{\beta}) + r_{\Delta y}(j,\boldsymbol{\beta}) + w r_{\Delta z}(j,\boldsymbol{\beta}) \tag{8}$$

where $w$ is a weighting component[2]. While there can be many ways to select $w$, a simple scheme was chosen as

$$w_z = \frac{1}{n_t}\sum_{j}^{n_t} \frac{\max\left(\Delta x(j)\right) + \max\left(\Delta y(j)\right)}{2\max\left(\Delta z(j)\right)} \tag{9}$$

which represents the ratio of the average $x$ and $y$ displacement to the maximum $z$ displacement. This resulted in $w = 0.1$ for the bulge inflation tests under consideration. This equation to weight displacement components differently is similar to a relative error formulation used by Yun et al. (2018), and also similar to normalization schemes used in multi-objective optimizations as described by Tam (2020).

The optimization requires the objective function to be computed multiple times in the FEMU procedure. There are many steps required to automate this using

[2] The software available online allows a weight to be specified for each directional component of the displacement field.

software which is described in Table 2. Several Python functions were created to interface with the the ABAQUS solver and post processor for this application. The function essentially returns the objective from an inputted candidate set of material parameters.

Table 2 Process to compute the objective function for given material parameters.

| Step | Description |
|---|---|
| 1 | Write the material model parameters to the ABAQUS input file |
| 2 | Run ABAQUS solver on the input file |
| 3 | Run ABAQUS post processor to export displacement field of FE model |
| 4 | Load the FE displacement field into memory |
| 5 | Compute the discrepancy between FE model and DIC data:<br>i) Linearly interpolate the FE model to match the pressures of the bulge test data<br>ii) Construct and evaluate RBFs to the FE model displacement field<br>iii) Compute either $e_z$ or $r_{\Delta x}$, $r_{\Delta y}$, and $r_{\Delta z}$ for each set of test data |
| 6 | Compute the final objective function of $e$ or $e_w$ |

## 2.4 Optimization

The inverse analysis is the process of finding the material parameters of the FE model to match the bulge inflation test data. The optimization problem can be stated as

$$\text{minimize:} \quad e(\boldsymbol{\beta}) \tag{10}$$

$$\text{subject to:} \quad \beta_l \leq \beta_k \leq \beta_u, \quad k = 1, 2, \cdots, n_p. \tag{11}$$

where $\boldsymbol{\beta}$ is the vector of material parameters which are restricted to some reasonable lower and upper bounds, and $e(\boldsymbol{\beta})$ represents some objective function describing the discrepancy between experiment and numerical model. Bounds will depend upon the material model, and in this case were selected to occur just beyond the observed range in Jekel et al. (2017). In cases where there is no previous literature on the material or material model, bounds can be selected based on the feasible domain of the FE model. For this FE model, there is some lower bound to the stiffness parameter which will cause the FE model not to converge, however such upper bound does not exists. The isotropic parameters are expressed as $\boldsymbol{\beta} = (E)$ or $\boldsymbol{\beta} = (E, G)$, and the simplified orthotropic parameters are expressed as $\boldsymbol{\beta} = (E_1, E_2, G_{12})$.

A multi-start optimization strategy was utilized in order to avoid the presence of multiple local minima. A variant of the BFGS (Broyden, 1970; Fletcher, 1970; Goldfarb, 1970; Shanno, 1970) gradient based optimization was used as the local optimizer (Virtanen et al., 2020; Byrd et al., 1995). The multi-start process ran five BFGS optimizations from different random starting points in the design space (Schutte et al., 2006). Each of the five BFGS runs were limited to either 200 function evaluations, or satisfying the convergence criteria. The convergence considered either relative changes in the objective function, absolute changes in the objective function, or gradient magnitude.

There is the possibility that some combination of material parameters may cause the FE analysis to not converge. As an exaggerated example, consider the case when

stiffness moduli approach zero. In such a case the deformation becomes too large that finite elements become poorly shaped and unable to converge. There were observed instances in our optimizations when the optimizer would try a material parameter combination that the FEM would fail to reach final convergence. The boundary of the feasible set of parameters that does not run into this type of FE issues is not known a priori. To deal with this problem, the maximum objective value from the run-time history was passed to the optimization algorithm when the FE analysis failed to converge.

While there were a number of potential issues using gradient based optimization with this application, in practice the gradient optimization was able to produce objective functions lower than an initial random guess. Looking at the optimization history, the FE analysis would only fail to converge during the line search stage of the gradient based optimization algorithm, and not the finite differences which was used to approximate gradients. Lastly, there were no observed issues with the optimization caused by the $L^1$ objective function, noting that the gradients won't exist if a zero objective value occurs.

## 3 Results

Inverse analyses were performed on the bulge inflation tests to find material parameters for the linear orthotropic model. The focus of the results is to demonstrate the effect of minimizing three different objective functions. These objective functions are summarized as the sum of full-field displacement residuals ($e$), the sum of weighted displacement full-field residuals ($e_w$), and the bulge height residual ($e_z$) which considered only a single point.

The simplified linear orthotropic material parameters resulting from inverse analysis on the individual tests are shown in Table 3. There are different material parameters depending upon which objective function was minimized. The most noticeable parameter differences can be seen in the primary $E_1$ and secondary $E_2$ stiffness moduli. The most interesting changes occur in the second and third test, where the choice of objective function reversed the stiffness directions. Minimizing $e$ or $e_z$ resulted in $E_2 > E_1$, but minimizing $e_w$ resulted in $E_1 > E_2$. Overall, minimizing $e_w$ resulted in parameters that were more consistent from test to test as evident by having the lowest range for the set of tests. As a reminder each test was conducted on a nominally identical material specimen, and it was expected that there would be minimum parameter differences from test to test. While $E_1$ and $E_2$ stiffness moduli were very different depending on $e$ or $e_w$, the shear modulus was nearly the same in all conditions.

The objective values resulting from each parameter set with the linear orthotropic model are shown in Table 4. The table shows the resulting values of $e_w$ and $e_z$ when $e$ was minimized, and vice versa. The definition of the worst fit depends upon which objective function was minimized. It is important to point out that for each test, the minimum value of each objective only occurred when that objective was minimized. If this was not the case, it would indicate that an optimization had failed because a better optimum existed. The other important aspect of this table is that it demonstrates that objective functions are fundamentally different. In other words, finding the best $e_z$ does not yield the best $e$ or $e_w$, and vice versa.

Table 3 Resulting orthotropic material parameters from minimizing tests independently with each inverse analysis. Note that $\nu_{12}$ was fixed to 0.24.

| | Minimizing $e$ (GPa) | | | Minimizing $e_w$ (GPa) | | | Minimizing $e_z$ (GPa) | | |
|---|---|---|---|---|---|---|---|---|---|
| | $E_1$ | $E_2$ | $G_{12}$ | $E_1$ | $E_2$ | $G_{12}$ | $E_1$ | $E_2$ | $G_{12}$ |
| Test 1 | 0.343 | 0.248 | 0.005 | 0.303 | 0.229 | 0.005 | 0.343 | 0.246 | 0.005 |
| Test 2 | 0.212 | 0.241 | 0.004 | 0.306 | 0.230 | 0.005 | 0.213 | 0.219 | 0.003 |
| Test 3 | 0.217 | 0.257 | 0.004 | 0.306 | 0.229 | 0.005 | 0.206 | 0.209 | 0.003 |
| Test 4 | 0.239 | 0.215 | 0.004 | 0.280 | 0.215 | 0.005 | 0.210 | 0.214 | 0.003 |
| Mean | 0.252 | 0.240 | 0.004 | 0.299 | 0.226 | 0.005 | 0.243 | 0.222 | 0.003 |
| Range | 0.131 | 0.042 | 0.001 | 0.026 | 0.015 | 0.000 | 0.137 | 0.037 | 0.002 |

Table 4 Objective values when minimizing $e$, $e_w$, or $e_z$ for each bulge inflation test.

| | Minimizing $e$ (GPa) | | | Minimizing $e_w$ (GPa) | | | Minimizing $e_z$ (GPa) | | |
|---|---|---|---|---|---|---|---|---|---|
| | $e$ | $e_w$ | $e_z$ | $e$ | $e_w$ | $e_z$ | $e$ | $e_w$ | $e_z$ |
| Test 1 | 1.55 | 0.51 | 1.75 | 1.77 | 0.49 | 2.81 | 1.55 | 0.51 | 1.75 |
| Test 2 | 1.66 | 0.77 | 1.03 | 1.92 | 0.71 | 2.25 | 1.78 | 0.83 | 0.86 |
| Test 3 | 1.70 | 0.57 | 2.04 | 1.76 | 0.53 | 2.71 | 2.19 | 0.74 | 0.71 |
| Test 4 | 1.03 | 0.41 | 0.82 | 1.10 | 0.38 | 1.27 | 1.11 | 0.45 | 0.76 |

The objective values were compared with a zero displacing FE model to draw comparison at a poor design point. This can be thought of as an much stiffer material model (i.e. two orders of magnitude larger), and represents the worst possible calibration for each test. Additionally, this could be used as the starting point for an optimization algorithm, because it should always be possible to select a material model that does not displace. The objective values are shown in Table 5, and can be seen to be approximately four times worse than the best optimized objective values. The different objective functions do not agree to which test has the best fit to the zero displacement model. The third test has the lowest $e$ and $e_z$ values, while the second test has the lowest $e_w$ value. Again, this demonstrates that objective functions are fundamentally different.

Table 5 Objective values for a zero displacement numerical model (infinitely stiff material).

| | $e$ | $e_w$ | $e_z$ |
|---|---|---|---|
| Test 1 | 5.62 | 2.03 | 3.99 |
| Test 2 | 5.59 | 1.53 | 4.51 |
| Test 3 | 4.50 | 1.67 | 3.14 |
| Test 4 | 5.75 | 1.74 | 4.76 |

Comparisons between the FE models and the test data are shown in Figure 7. The figures show slices along the lines $y = 0$ and $x = 0$ at a selected inflation pressure. The mean squared error (mse) is shown in each figure, which can be used to quantify which result best matches the experimental data. The results from other inflation pressures are qualitatively similar to the differences in objective functions shown here. Additionally, figures from all inflation pressures as well as inflation videos are included in the supplementary material. In general the FE models had a tendency to overestimate the deflection at low pressures, but underestimate the deflection at high pressures.

It appears that the objective function $e_z$ matches the apex of the bulge test better than $e$ or $e_w$. The apex is where the largest $\Delta z$ deflection occurs, and it appears that

$e$ is much better at matching the apex than $e_w$. While $e_w$ does a poor job matching the deflections at the apex, it potentially does a better job of matching the profile (or shape) of the bulge inflation test along the outer edges of the test ($|x| \geq 50$ and $|y| \geq 50$). It can be noted that the results from $e$ and $e_z$ are more similar, while the results from $e_w$ appears to be the most different.

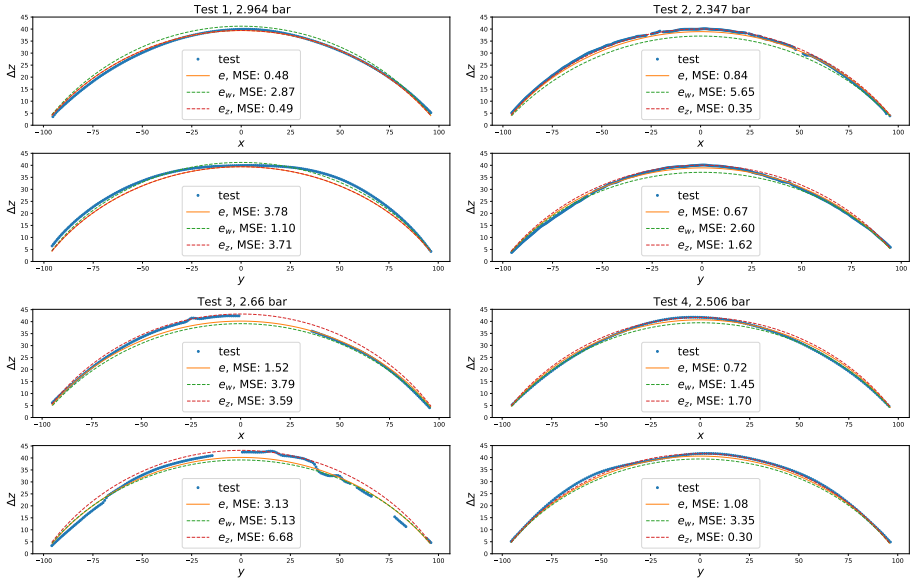


Fig. 7 Profiles through the lines $y = 0$ and $x = 0$ comparing the results using each objective function for the four tests.

The previous figures highlighted the $\Delta z$ displacements. This is the most intuitive displacement component, as $\Delta z$ resembles the shape one sees while performing this test. However, $\Delta z$ is only one-third of the displacement components. Profiles of $\Delta x$ and $\Delta y$ are shown in Figure 8. The $\Delta x$ displacement was plotted along the line $y = 0$, and the $\Delta y$ displacement along the line $x = 0$. These profiles cut through the interesting behavior of the maximum in-plane deformations, which somewhat resemble a sinusoidal wave. Again a lower mse means the result is a better match to the experimental data. The same inflation pressures form the previous figures are highlighted.

It should not be a surprise to report that the $e_w$ objective function matches the $\Delta x$ and $\Delta y$ displacements better than the other objective functions. Essentially $e_w$ puts more importance on matching the in-plane displacement components correctly, and as a result the peaks of the $\Delta x$ and $\Delta y$ displacement are better represented with $e_w$. While the results for $e_z$ and $e$ are similar, a slight edge can be given to $e$ as it appears to matches the $\Delta x$ and $\Delta y$ slightly better than $e_z$ through the shown inflation pressures.

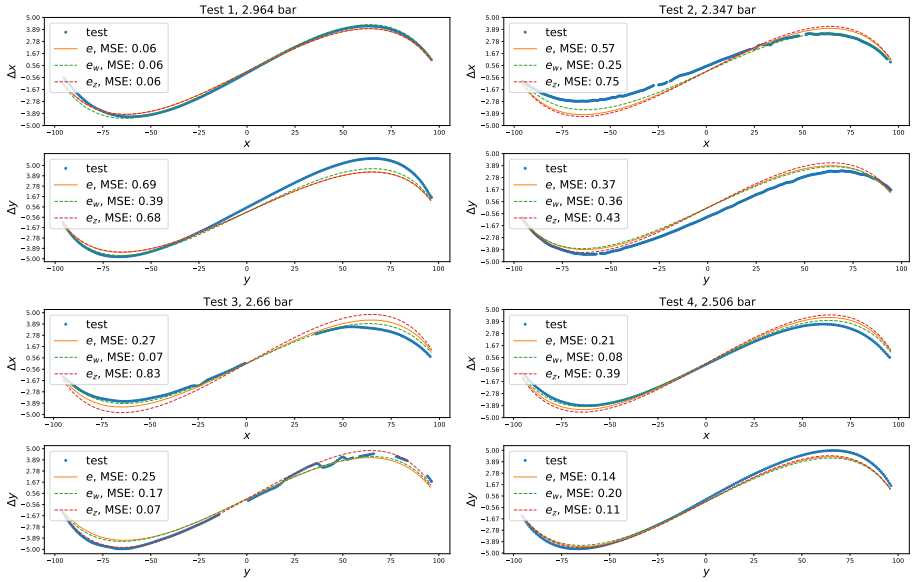


Fig. 8 Profiles of $\Delta x$ and $\Delta y$ through the lines $y = 0$ and $x = 0$ comparing the results using each objective function.

## 4 Discussion

The results characterized the $E_1$, $E_2$, and $G_{12}$ stiffness moduli from a bulge inflation test. Fundamentally these material components all lie in the material plane, however the bulge test is likely to produce larger out-of-plane than in-plane displacements. The different objective functions compare three cases: i) only matching the maximum out-of-plane displacement ($e_z$), ii) all displacement components equally ($e$), and iii) a weighted balance between in-plane and out of plane components ($e_w$).

The most striking result was the effect of the objective functions on selecting parameters for the linear orthotropic material model. When $e$ or $e_z$ was minimized the linear orthotropic parameters varied significantly from test to test, with some tests resulting in $E_2 > E_1$ and others $E_1 > E_2$. This was not the case when $e_w$ was minimized, in which the parameters from test to test were consistent with $E_1 > E_2$. We know that $E_1 > E_2$ given our understanding of the material's construction and manufacturer's statements. Additionally, the results from $e_w$ better match quasi-static uniaxial tests for $E_2$ performed by Jekel et al. (2017). These tests show that $E_1 \approx 0.3$ and $E_2 \approx 0.2$ at 0.1 strain, which agree well with the $e_w$ results presented here.

It's important to clarify that $e_z$, $e$, and $e_w$ would all approach zero if it was possible for a perfect fit to the experimental data. Given that the model was incapable of a perfect fit, we obtained different material model parameters depending upon objective function which each quantify the best fit differently. This demonstrates the importance of full-field data over single point data for a complicated load-case, as characterizing only the maximum deflection point was unable to accurately characterize the $E_1$ and $E_2$ moduli. This work also demonstrates that work with full 3D field data may need to take special consideration of objective functions. Despite $e$

considering the full-field data, it resulted in nearly the same parameters as $e_z$ which only consider a single point, because of the dominance of the $\Delta z$ displacements.

Test 2 and Test 3 are of particular interest with the linear orthotropic model, because these tests resulted in $E_2 > E_1$ when $e$ was minimized. It could be reasonable to assume that the test directions were incorrect by a factor of 90°, and that this mistake in the $x$ and $y$ directions resulted in the set of parameters. Additional inverse analyses were performed on these tests, where the test data was rotated by factors of 45° and 90°. What is interesting is that when $e$ was minimized the resulting parameters resulted in $E_2 > E_1$ regardless of the rotation, and there was little change to the parameters. However, when $e_w$ was minimized both $E_2$ and $E_1$ would change significantly based on the rotation. This hints that giving more weight to the $x$ and $y$ displacements, like in $e_w$, would be better if an inverse analyses was required to identify orthotropic parameters without knowing the primary and secondary material directions.

The linear orthotropic material in the FE model appears to be provide a reasonable representation of the test data. One of the benefits of the formulation of the $e$ objective function is that it's value is an easily interpretable physical length (as opposed to an $L^2$ norm). Here the largest value of $e$ seen in table 4 was about 2 mm, so the average deviation between of all models and experiments was a Manhattan distance less than 2 mm.

## 5 Conclusion

An inverse analysis was described to find material parameters by matching the full displacement field from bulge inflation tests. Optimization was used to find material parameters in a FE model that best matched the experimental displacement field from tests on PVC-coated polyester. Material parameters were determined for a simplified linear orthotropic material model. Three different objective functions were considered to describe the discrepancy between the experimental data and numerical model. One objective function considered only a single point, another considered the full 3D displacement field, and the last objective function considered a weighted residual of the full displacement field. The weighting scheme was chosen to compensate for the fact that the majority of the deflections within the bulge inflation test occur out-of-plane, and thus weighted the out-of-plane deflections equal to the in-plane deflections. Resulting material parameters for the linear orthotropic material model were very different depending on which objective function was minimized. Thus the choice of objective function being considered is very important when performing such an optimization on the full-field data. The definitions of the simplified orthotropic material parameters occur in the material plane. Matching only the maximum single out-of-plane bulge deflection, or matching the full 3D displacement components resulted in similar material parameters that were thought to be invalid. The resulting in-plane stiffness moduli calibrated were potentially non-physical. However, better in-plane stiffness moduli were identified when the in-plane deflections were weighted equal to the out-of-plane deflections using the full-field measurements. This hopefully serves as an important lesson when working with full-field data that has one or two dominating components, as potentially the smaller value measurements may be significantly more important.

Acknowledgements Thanks to Sudharshan Udhayakumar for help constructing the FE model and comparing the FE model to analytical solutions. Thanks to Andrés Bernardo for helping set up the script to process the full displacement field data. We are grateful to the anonymous reviewers who have provided a number of comments that greatly improved the quality of this manuscript.

## Replication of results

The FE models require a commercial code to run. Experimental data, Python scripts to perform the optimization, and FE model input decks are available online with instructions at `https://github.com/cjekel/inv_bubble_opt`

## Declarations

### Funding

Charles F. Jekel has received the following funding for his PhD research which has supported this work: University of Florida Graduate Preeminence Award, U.S. Department of Veterans Affairs Educational Assistance, and Stellenbosch University Merrit Bursary.

### Conflicts of interest

The authors declare that they have no conflict of interest.

### Availability of data and material

The experimental data is available online with instructions on how to download at `https://github.com/cjekel/inv_bubble_opt`

### Code availability

The scientific Python ecosystem was used to produce these results. Specific scripts used to perform the optimizations are available online at `https://github.com/cjekel/inv_bubble_opt`

## References

Ambroziak A, Kłosowski P (2014) Mechanical properties for preliminary design of structures made from PVC coated fabric. Construction and Building Materials 50:74–81, DOI 10.1016/j.conbuildmat.2013.08.060

Asaadi E, Wilke DN, Heyns PS, Kok S (2017) The use of direct inverse maps to solve material identification problems: pitfalls and solutions. Structural and Multidisciplinary Optimization 55(2):613–632, DOI 10.1007/s00158-016-1515-1, URL `https://doi.org/10.1007/s00158-016-1515-1`

Broomhead DS, Lowe D (1988) Radial basis functions, multi-variable functional interpolation and adaptive networks. Tech. rep., Royal Signals and Radar Establishment Malvern (United Kingdom)

Broyden CG (1970) The Convergence of a Class of Double-rank Minimization Algorithms 1. General Considerations. IMA Journal of Applied Mathematics 6(1):76–90, DOI 10.1093/imamat/6.1.76, URL https://dx.doi.org/10.1093/imamat/6.1.76

Byrd RH, Lu P, Nocedal J, Zhu C (1995) A limited memory algorithm for bound constrained optimization. SIAM Journal on Scientific Computing 16(5):1190–1208

Cailletaud G, Pilvin P (1994) Identification and inverse problems related to material behaviour. Inverse problems in engineering mechanics 1:79–86

Charalambides M, Wanigasooriya L, Williams G, Chakrabarti S (2002) Biaxial deformation of dough using the bubble inflation technique. I. Experimental. Rheologica Acta 41(6):532–540, DOI 10.1007/s00397-002-0242-2

Conte SD, Boor CWD (1980) Elementary Numerical Analysis: An Algorithmic Approach, 3rd edn. McGraw-Hill Higher Education

Dinh TD, Rezaei A, Daelemans L, Mollaert M, Hemelrijck DV, Paepegem WV (2017) A hybrid micro-meso-scale unit cell model for homogenization of the nonlinear orthotropic material behavior of coated fabrics used in tensioned membrane structures. Composite Structures 162:271–279, DOI https://doi.org/10.1016/j.compstruct.2016.12.027, URL http://www.sciencedirect.com/science/article/pii/S0263822316313204

Drass M, Schneider J (2016) On the mechanical behavior of transparent structural silicone adhesive–TSSA. In: SEMC 2016–Sixth International Conference on Structural Engineering, Mechanics and Computation, pp 14–16

Fletcher R (1970) A new approach to variable metric algorithms. The Computer Journal 13(3):317–322, DOI 10.1093/comjnl/13.3.317, URL https://dx.doi.org/10.1093/comjnl/13.3.317

Galliot C, Luchsinger R (2009) A simple model describing the non-linear biaxial tensile behaviour of PVC-coated polyester fabrics for use in finite element analysis. Composite Structures 90(4):438–447, DOI 10.1016/j.compstruct.2009.04.016

Goldfarb D (1970) A family of variable-metric methods derived by variational means. Math Comp 24 (1970), 23-26 DOI https://doi.org/10.1090/S0025-5718-1970-0258249-6

Jekel CF (2016) Obtaining non-linear orthotropic material models for PVC-coated polyester via inverse bubble inflation. Master's thesis, Stellenbosch University, URL http://hdl.handle.net/10019.1/98627

Jekel CF, Venter G, Venter MP (2016) Obtaining a hyperelastic non-linear orthotropic material model via inverse bubble inflation analysis. Structural and Multidisciplinary Optimization pp 1–9, DOI 10.1007/s00158-016-1456-8, URL http://dx.doi.org/10.1007/s00158-016-1456-8

Jekel CF, Venter G, Venter MP (2017) Modeling PVC-coated polyester as a hypoelastic non-linear orthotropic material. Composite Structures 161:51–64, DOI http://dx.doi.org/10.1016/j.compstruct.2016.11.019, URL http://www.sciencedirect.com/science/article/pii/S0263822316320839

Jekel CF, Venter G, Venter MP, Stander N, Haftka RT (2019) Similarity measures for identifying material parameters from hysteresis loops using inverse analysis. International Journal of Material Forming 12(3):355–378, DOI 10.1007/s12289-018-1421-8, URL https://doi.org/10.1007/s12289-018-1421-8

Jung BC, Yoon H, Oh H, Lee G, Yoo M, Youn BD, Huh YC (2016) Hierarchical model calibration for designing piezoelectric energy harvester in the presence of variability in material properties and geometry. Structural and Multidisciplinary Optimization 53(1):161–173, DOI 10.1007/s00158-015-1310-4, URL https://doi.org/10.1007/s00158-015-1310-4

LaVision GmbH (2014) Product-Manual DaVis 8.2 Software, 8th edn. Göttingen, Germany

Lee G, Kim W, Oh H, Youn BD, Kim NH (2019) Review of statistical model calibration and validation—from the perspective of uncertainty structures. Structural and Multidisciplinary Optimization 60(4):1619–1644, DOI 10.1007/s00158-019-02270-2, URL https://doi.org/10.1007/s00158-019-02270-2

Lovato G, Moret F, Le Gallo P, Cailletaud G, Pilvin P (1993) Determination of brazed joint constitutive law by inverse method. Le Journal de Physique IV 3(C7):C7—-1135

Machado G, Favier D, Chagnon G (2012) Membrane curvatures and stress-strain full fields of axisymmetric bulge tests from 3D-DIC measurements. Theory and validation on virtual and experimental results. Experimental mechanics 52(7):865–880

Oh H, Kim J, Son H, Youn BD, Jung BC (2016) A systematic approach for model refinement considering blind and recognized uncertainties in engineered product development. Structural and Multidisciplinary Optimization 54(6):1527–1541

Rachik M, Schmidtt F, Reuge N, Le Maoult Y, Abbeé F (2001) Elastomer biaxial characterization using bubble inflation technique. II: Numerical investigation of some constitutive models. Polymer Engineering & Science 41(3):532–541, DOI 10.1002/pen.10750, URL https://onlinelibrary.wiley.com/doi/abs/10.1002/pen.10750

van Rensburg GJJ, Kok S, Wilke DN (2018) Simultaneous estimation of boundary conditions and material model parameters. Structural and Multidisciplinary Optimization 58(2):701–717

Reuge N, Schmidt FM, Le Maoult Y, Rachik M, Abbé F (2001) Elastomer biaxial characterization using bubble inflation technique. I: Experimental investigations. Polymer Engineering and Science 41(3):522–531, DOI 10.1002/pen.10749

Sasso M, Palmieri G, Chiappini G, Amodio D (2008) Characterization of hyperelastic rubber-like materials by biaxial and uniaxial stretching tests based on optical methods. Polymer Testing 27(8):995–1004, DOI 10.1016/j.polymertesting.2008.09.001, URL http://www.sciencedirect.com/science/article/pii/S0142941808001529

Schutte JF, Haftka RT, Fregly BJ (2006) Improved global convergence probability using multiple independent optimizations. International Journal for Numerical Methods in Engineering 71(6):678–702, DOI 10.1002/nme.1960, URL https://doi.org/10.1002/nme.1960

Shanno DF (1970) Conditioning of quasi-Newton methods for function minimization. Math Comp 24 (1970), 647-656 DOI https://doi.org/10.1090/S0025-5718-1970-0274029-X

Shaw A, Sriramula S, Gosling PD, Chryssanthopoulos MK (2010) A critical reliability evaluation of fibre reinforced composite materials based on probabilistic micro and macro-mechanical analysis. Composites Part B: Engineering 41(6):446–453, DOI https://doi.org/10.1016/j.compositesb.2010.05.005, URL http://www.sciencedirect.com/science/article/pii/S1359836810000818

Sheplak M, Dugundji J (1998) Large Deflections of Clamped Circular Plates Under Initial Tension and Transitions to Membrane Behavior. Journal of Applied Mechanics 65(1):107–115, URL http://dx.doi.org/10.1115/1.2789012

Son H, Lee G, Kang K, Kang YJ, Youn BD, Lee I, Noh Y (2020) Industrial issues and solutions to statistical model improvement: a case study of an automobile steering column. Structural and Multidisciplinary Optimization pp 1–18

Stranghöner N, Uhlemann J, Bilginoglu F, Bletzinger KU, Bögner-Balz H, Corne E, Gibson N, Gosling P, Houtman R, Llorens J, Others (2016) Prospect for European Guidance for the Structural Design of Tensile Membrane Structures. Science and Policy Report (SaP-Report) Draft Version To be published by the Joint Research Centre (JRC) of the European Commission, publication expected

Tam JH (2020) Identification of elastic properties utilizing non-destructive vibrational evaluation methods with emphasis on definition of objective functions: a review. Structural and Multidisciplinary Optimization DOI 10.1007/s00158-019-02433-1, URL https://doi.org/10.1007/s00158-019-02433-1

Tonge TK, Atlan LS, Voo LM, Nguyen TD (2013a) Full-field bulge test for planar anisotropic tissues: Part I – Experimental methods applied to human skin tissue. Acta Biomaterialia 9(4):5913–5925, DOI https://doi.org/10.1016/j.actbio.2012.11.035, URL http://www.sciencedirect.com/science/article/pii/S1742706112005983

Tonge TK, Voo LM, Nguyen TD (2013b) Full-field bulge test for planar anisotropic tissues: Part ii – a thin shell method for determining material parameters and comparison of two distributed fiber modeling approaches. Acta Biomaterialia 9(4):5926–5942, DOI https://doi.org/10.1016/j.actbio.2012.11.034, URL https://www.sciencedirect.com/science/article/pii/S1742706112005843

Virtanen P, Gommers R, Oliphant TE, Haberland M, Reddy T, Cournapeau D, Burovski E, Peterson P, Weckesser W, Bright J, van der Walt SJ, Brett M, Wilson J, Jarrod Millman K, Mayorov N, Nelson ARJ, Jones E, Kern R, Larson E, Carey C, Polat I, Feng Y, Moore EW, Vand erPlas J, Laxalde D, Perktold J, Cimrman R, Henriksen I, Quintero EA, Harris CR, Archibald AM, Ribeiro AH, Pedregosa F, van Mulbregt P, Contributors S (2020) SciPy 1.0: Fundamental Algorithms for Scientific Computing in Python. Nature Methods DOI https://doi.org/10.1038/s41592-019-0686-2

Yun W, Lu Z, Jiang X (2018) A modified importance sampling method for structural reliability and its global reliability sensitivity analysis. Structural and Multidisciplinary Optimization 57(4):1625–1641

Zhan Z, Fu Y, Yang RJ, Peng Y (2011) An automatic model calibration method for occupant restraint systems. Structural and Multidisciplinary Optimization 44(6):815–822, DOI 10.1007/s00158-011-0671-6, URL https://doi.org/10.1007/s00158-011-0671-6